

# Effect of a Mutation on the Structure and Dynamics of an $\alpha$ -Helical Antifreeze Protein in Water and Ice

Steffen P. Graether, Carolyn M. Slupsky, and Brian D. Sykes\*

CIHR Group in Protein Structure and Function, Department of Biochemistry and Protein Engineering Network of Centres of Excellence, University of Alberta, Edmonton, Canada

**ABSTRACT** One strategy of psychrophilic organisms to survive subzero temperature is to produce antifreeze protein (AFPs), which inhibit the growth of macromolecular ice. To better understand the binding mechanism, the structure and dynamics of several AFPs have been studied by nuclear magnetic resonance (NMR) and X-ray crystallography. The results have shown that different organisms can use diverse structures ( $\alpha$ -helix,  $\beta$ -helix, or different globular folds) to achieve the same function. A number of studies have focused on understanding the relationship between the  $\alpha$ -helical structure of fish type I AFP and its function as an inhibitor of ice growth. The results have not explained whether the 90% activity loss caused by the conservative mutation of two threonines to serines (Thr13Ser/Thr24Ser) is attributable to a change in protein structure in solution or in ice. We examine here the structure and dynamics of the winter flounder type I AFP and the mutant Thr13Ser/Thr24Ser in both solution and solid states using a wide range of NMR approaches. Both proteins remain fully  $\alpha$ -helical at all temperatures and in ice, demonstrating that the activity change must therefore not be attributable to changes in the protein fold or dynamics but differences in surface properties. *Proteins* 2006;63:603–610. © 2006 Wiley-Liss, Inc.

**Key words:** chemical shift; growth inhibition; NMR; solid-state; winter flounder

## INTRODUCTION

The formation of macromolecular ice in an organism can cause physical damage through shear stress on membranes and the loss of protein function through dehydration. Some organisms are able to survive subzero temperatures by producing antifreeze proteins (AFPs, also known as thermal hysteresis proteins or ice-structuring proteins). AFPs prevent the formation of macroscopic ice crystals by inhibiting the growth of small ice crystals,<sup>1</sup> and/or by masking heterogeneous nucleating sites.<sup>2</sup> The inhibition of ice crystal growth is thought to occur through the Kelvin effect, where the binding of AFP causes the ice between the bound proteins to grow as a curved front, which is an energetically unfavorable process.<sup>3</sup> The Kelvin effect results in a nonequilibrium depression of the freezing point below the melting point; the difference between the two temperatures is defined as thermal hysteresis (TH), and is

used to measure the antifreeze activity of a protein. Early models proposed that this binding must be irreversible in order to completely inhibit ice growth. Recent experimental results, however, show that the protein is able to adsorb and desorb from the surface.<sup>4</sup> These authors suggest that AFPs do not work by the Kelvin effect, but instead form a decreasing concentration gradient away from the ice surface, which creates a dense layer of AFPs that depress the freezing point through a local colligative effect.<sup>4</sup>

It has been a greater challenge to characterize the interaction between AFP and ice at the atomic level. Widely diverse AFP structures have been determined from fish and insects (for reviews, see Refs. 5–10), such that no comprehensive structural motif has emerged for this family of proteins. Nevertheless, the winter flounder HPLC isoform 6 type I AFP is used as a model for this protein class. Type I AFP is 37 amino acids long, of which 23 residues are alanines. The structure of type I AFP has been shown to be a single  $\alpha$ -helix with cap structures at the termini.<sup>11,12</sup> Four Thr residues are spaced 11 residues apart on the same side of the helix (Fig. 1). Analysis of the X-ray structure and ice-binding properties led to the hypothesis that the protein binds to a specific plane of ice through hydrogen bonds from the threonyl hydroxyl (Thr2, Thr13, Thr24, and Thr35).<sup>11,13–15</sup> Further experimentation, however, has shown that the hydroxyl moiety is not critical to ice binding. Mutagenesis of the two central or all four threonines to serines (TTTT to TSST or SSSS), which preserves the hydrogen bonding potential of the side-chain, caused a 90–100% loss in activity relative to the

The Supplementary Material referred to in this article can be found at <http://www.interscience.wiley.com/jpages/0887-3585/suppmat/>

**Abbreviations:** AFP, antifreeze proteins; DSS, 2,2'-dimethyl-2-silapentane-5-sulfonate; MAS, magic-angle spinning; TH, thermal hysteresis.

Grant sponsor: CIHR; Grant sponsor: Government of Canada's Network of Centres of Excellence program (supported by CIHR and NSERC through the Protein Engineering Network of Centres of Excellence, Inc.).

Steffen P. Graether's present address is Department of Molecular and Cellular Biology, University of Guelph, Guelph, Ontario, N1G 2W1 Canada.

\*Correspondence to: Brian D. Sykes, 419 Medical Sciences Building, University of Alberta, Edmonton AB T6G 2H7. E-mail: brian.sykes@ualberta.ca

Received 8 August 2005; Revised 2 November 2005; Accepted 7 November 2005

Published online 25 January 2006 in Wiley InterScience ([www.interscience.wiley.com](http://www.interscience.wiley.com)). DOI: 10.1002/prot.20889

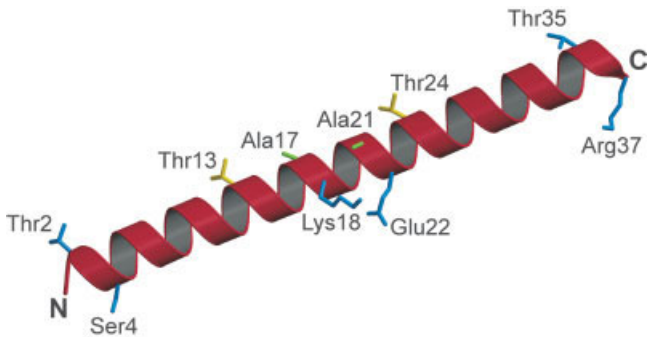


Fig. 1. Structure of type I AFP. A ribbon representation of the  $\alpha$ -helical protein with key residues shown in stick representation. The locations of the mutations (Thr13Ser and Thr24Ser) are shown in yellow. Residues examined by liquid-state  $^{13}\text{C}$  dynamics (Thr2, Ser4, Lys18, Glu22, Thr35, and Arg37) are shown in blue. The locations of the  $^{13}\text{C}\alpha$  label used in the  $^{13}\text{C}$  solid-state studies of wild-type ( $^{13}\text{C}\alpha$ -Ala17) and TSST ( $^{13}\text{C}\alpha$ -Ala21) are colored green. The wild-type sequence and three-dimensional structure are from PDB entry 1wfb.

wild-type protein.<sup>16–18</sup> Mutation of the two threonines to valines, which preserves the isosteric nature of the side-chain but not the potential hydrogen bond, resulted in only a moderate loss in activity (0–15% loss).<sup>16–18</sup> An additional problem with the hydrogen-bonding model is that it is not able to explain the preferential binding of the protein to ice rather than water. Theoretically, hydrogen bonds should form more favorably between water and ice or water and protein than between ice and protein, given that water is able to orient itself to form “perfect” hydrogen bonds.<sup>19</sup> The structural studies of type I AFP showed that threonine hydroxyl group would likely preferentially bind to the backbone rather than ice.<sup>11,20</sup> This series of mutagenesis and structural experiments demonstrate that the threonyl hydroxyl is not an essential requirement for ice binding.

The reduced importance of hydrogen bonds in ice binding has led to the exploration of the role of methyl groups of the threonine and alanine residues. Mutation of Ala17, a residue adjacent to the Thr-rich face, to Leu was shown to abolish all antifreeze activity.<sup>21</sup> This led the authors to propose that the ice-binding face of type I AFP consists of the alanine-rich face along with the Thr  $\gamma$ -methyl of the four threonines (Thr2, Thr13, Thr24, and Thr35). Support for the importance of the  $\gamma$ -methyls has come from studies using allo-Thr, the stereoisomer of the Thr side-chain.<sup>18</sup> It was demonstrated that when the four threonines are replaced with allo-Thr, type I AFP has no activity at a protein concentration of 1 mM. It has been suggested that van der Waals interactions, sometimes termed “shape complementarity,” may drive the binding of AFP to the ice surface.<sup>9,21,22</sup> Another proposal, resulting from two separate computational studies, suggests that desolvation of hydrophobic groups is the main contributor to the free energy of binding.<sup>23,24</sup> However, these new hypotheses are not yet able to explain all aspects of the interaction. They do not explain why AFPs bind to certain planes of ice because these van der Waals interactions are not geometrically constrained as hydrogen bonds would be. The hypotheses also assume that the structures of wild-type and

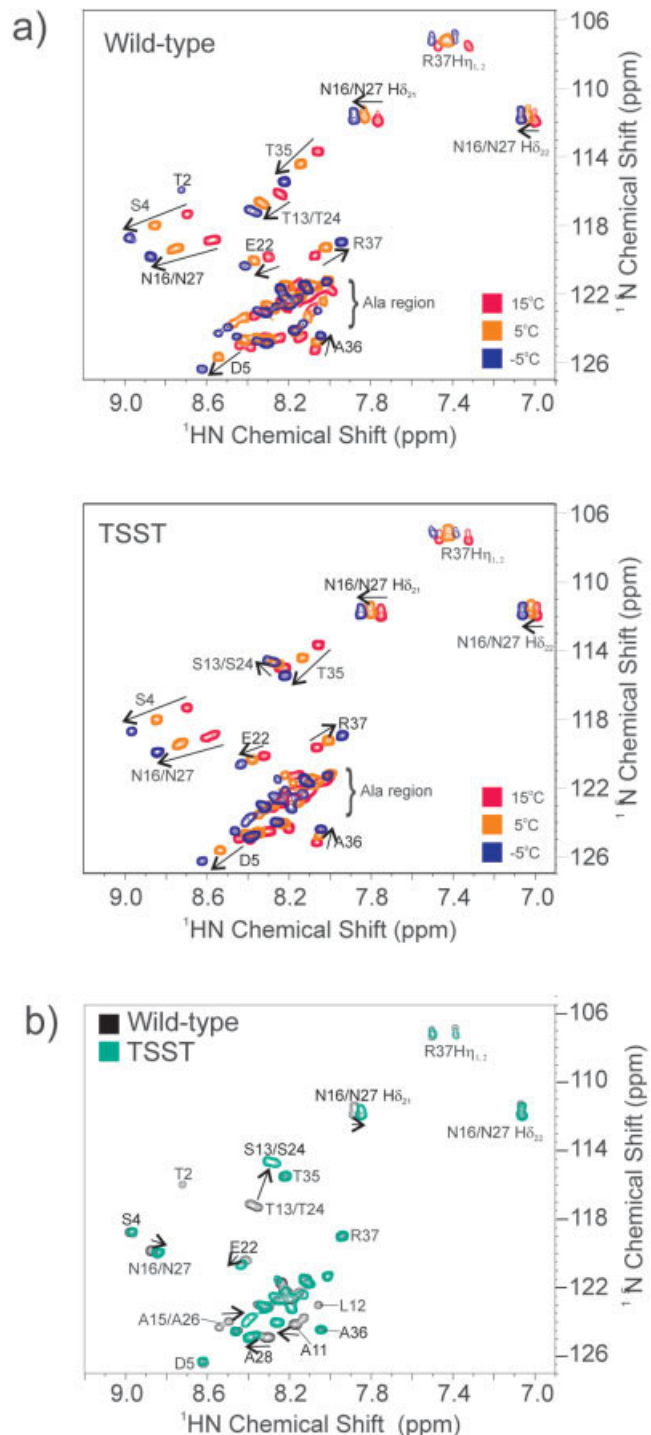


Fig. 2. Comparison of the structure of wild-type and mutant TSST type I AFP using  $^1\text{H}$ - $^{15}\text{N}$  HSQC. **a**: Overlap of natural abundance  $^1\text{H}$ - $^{15}\text{N}$  HSQC NMR spectra at temperatures of 15, 5, and  $-5^\circ\text{C}$  of wild-type protein (top panel) and TSST (bottom panel). **b**: Overlap of natural abundance  $^1\text{H}$ - $^{15}\text{N}$  HSQC spectra of wild-type and TSST mutant type I AFP at  $-5^\circ\text{C}$ . The identity and chemical shift changes of well-resolved resonances are indicated with labels and arrows, respectively.

mutant AFP in ice are identical to that determined by X-ray crystallography and nuclear magnetic resonance (NMR), which has not been demonstrated.

To further investigate the molecular binding mechanism of AFP for ice and the role of methyl groups, we characterize the structure and dynamics of AFP in ice and in water. We had previously attempted to examine the structure of frozen type I AFP, but found that the high concentrations of protein required for NMR studies and repeated freeze/thaw cycles resulted in the formation of amyloid-like fibrils.<sup>25</sup> In this study, the concentration of protein has been lowered from 75 to 25 mg/mL and unnecessary temperature cycling has been eliminated to prevent fibril formation. We compare the behavior of wild-type type I AFP and the mutant Thr13Ser/Thr24Ser (TSST) in both solution and in ice using a wide variety of NMR approaches to examine whether the mutant has a lower thermal hysteresis activity because of changes in its  $\alpha$ -helical structure, differences in its dynamics, or changes in its surface properties.

## MATERIALS AND METHODS

The wild-type and mutant winter flounder HPLC-6 proteins were synthesized according to standard solid-phase peptide synthesis methods as described previously.<sup>26</sup> For  $^{13}\text{C}$ -labeled samples, a  $^{13}\text{C}$  $\alpha$ -alanine residue ( $2\text{-}^{13}\text{C}$ -alanine; Cambridge Isotopes Laboratories, Andover, MA) was incorporated at position 17 for the wild-type protein and at position 21 for the TSST mutant.

$^1\text{H}$ ,  $^{13}\text{C}$ , and  $^{15}\text{N}$  referencing in all NMR experiments was performed relative to a 2,2'-dimethyl-2-silapentane-5-sulfonate (DSS) standard as described.<sup>27</sup> Solution-state experiments were performed on a 4.7 mM (wild-type) or 5.6 mM (TSST) sample in 90%  $\text{H}_2\text{O}/\text{D}_2\text{O}$ , pH 5.5 in a medium-walled tube (524-PP-8; Wilmad, Buena, NJ). Natural abundance  $^{15}\text{N}$ -heteronuclear single quantum coherence (HSQC)<sup>28,29</sup> experiments were collected on a Varian Unity 600-MHz spectrometer (Palo Alto, CA) equipped with a triple-resonance probe and  $z$ -axis pulsed field gradients at 15, 5, and  $-5^\circ\text{C}$ . For these experiments, 448 ( $^1\text{H}$ N), and 64 ( $^{15}\text{N}$ ) complex data points were acquired with a total of 3,008 transients per  $t_1$  increment using spectral widths of 7,000.4 ( $^1\text{H}$ N) and 2,100.0 ( $^{15}\text{N}$ ) Hz. Natural abundance  $^{13}\text{C}$ -HSQC spectra were collected on identical equipment at  $5^\circ\text{C}$  by acquiring 512 ( $^1\text{H}$ ) and 298 ( $^{13}\text{C}$ ) complex data points with a total of 56 transients per  $t_1$  increment using spectra widths of 7,000.4 ( $^1\text{H}$ ) and 10,526.3 ( $^{13}\text{C}$ ) Hz. Nuclear Overhauser effect enhancement spectroscopy (NOESY)<sup>30</sup> and total correlation spectroscopy (TOCSY)<sup>31</sup> experiments were collected on a Varian INOVA 800-MHz spectrometer equipped with a triple-resonance probe and  $x$ -,  $y$ -, and  $z$ -axis pulsed field gradients at  $15^\circ$  and  $5^\circ\text{C}$ . For the NOESY experiments, 2,048 ( $^1\text{H}$  F1), and 512 ( $^1\text{H}$  F2) complex data points were acquired with 32 transients using spectral widths of 10,000 Hz in both dimensions. For the TOCSY experiments, 2,048 ( $^1\text{H}$  F1), and 256 ( $^1\text{H}$  F2) complex data points were acquired with 16 transients using spectral widths of 10,000 Hz in both dimensions.

Natural abundance  $^{13}\text{C}$ - $T_1$ ,  $^{13}\text{C}$ - $T_2$ , and  $\{^1\text{H}\}$ - $^{13}\text{C}$ -NOE NMR relaxation data were collected at  $5^\circ$  and  $-1.2^\circ\text{C}$  on a 4.7 mM sample of wild-type or TSST type I AFP in 99.9%

$\text{D}_2\text{O}$ , pH 5.5, using a medium-walled tube (524-PP-8; Wilmad). The Varian Unity 600-MHz spectrometer was equipped with a triple-resonance probe and a  $z$ -axis pulsed field gradient. The sensitivity enhanced  $^{15}\text{N}$ -HSQC pulse sequence developed by Farrow et al.<sup>32</sup> was adjusted in-house for  $^{13}\text{C}$ . Sweepwidths of 7,000.35 Hz ( $^1\text{H}$ ) and 3,318.68 Hz ( $^{13}\text{C}$ ) were used. For the  $^{13}\text{C}$ - $R_1$  and  $^{13}\text{C}$ - $R_2$  experiments, 448 ( $^1\text{H}$ ) and 48 ( $^{13}\text{C}$ ) complex data points were collected with 120 transients per increment with a recycle delay of 4.0 s. With respect to  $^{13}\text{C}$ - $R_1$  experiments, relaxation delays of 10.15, 50.75, 91.35, 172.55, 253.75, 456.75, and 619.15 ms were applied. For the  $^{13}\text{C}$ - $R_2$  experiments, relaxation delays of 16.34, 32.68, 49.02, 65.36, 81.70, 98.04, 114.38, and 130.72 ms were applied. The  $\{^1\text{H}\}$ - $^{13}\text{C}$  steady-state NOE experiments<sup>32</sup> were measured from two HSQC spectra collected with and without  $^1\text{H}$  saturation applied before the  $^{13}\text{C}$  excitation pulse, using recycle delays of 2 s (with 3 s of saturation) or 5 s (without saturation) and 256 transients. Relaxation data analysis was performed using the NMRView program<sup>33</sup> following the method outlined by Gagné et al.<sup>34</sup> The NOE ratio is defined as the intensity of the saturated NOE peak over the intensity of the peak without saturation.

For the solid-state NMR experiments, the spectra were collected at 7.04 Tesla (corresponding to a  $^1\text{H}$  Larmor frequency of 299.916 MHz and a  $^{13}\text{C}$  Larmor frequency of 75.416 MHz) on a wide-bore (89 mm) Varian Unity spectrometer equipped with a Varian/Chemagnetics double-resonance magic-angle spinning (MAS) probe. The 5.0-mm PENCIL-I MAS rotor was spun at 3.333 kHz and the temperature was maintained using a Chemagnetics temperature controller. Temperature calibration was performed to compensate for heating caused by MAS by using 100% methanol as an internal NMR thermometer.<sup>35,36</sup> Spinning at 3.333 kHz raises the temperature of the sample an average of  $2.8^\circ\text{C}$ . The lyophilized wild-type or TSST type I AFP was dissolved at 25 mg/mL in 99.9%  $\text{D}_2\text{O}$ . The solution was frozen overnight by spinning the sample at 3.333 kHz at  $-5.0^\circ\text{C}$  (corrected temperature). For the  $^{13}\text{C}$ -CP/MAS experiments, the cross-polarization contact time was 3.0 ms during which the  $^1\text{H}$  decoupling field strength was 78 kHz. During acquisition, the decoupling field strength was reduced to 55 kHz. The proton  $90^\circ$  pulsewidth was calibrated to be 3.6  $\mu\text{s}$ ; 13,312 transients were collected with a recycle delay of 5 s. For the  $^{13}\text{C}$ -MAS experiments, a  $^1\text{H}$  decoupler field strength of 16 kHz was applied to 1,024 transients with a recycle delay of 3 s.  $^{13}\text{C}$ -MAS and  $^{13}\text{C}$ -CP/MAS experiments were collected with 2,972 complex data points and a sweepwidth of 37,140 Hz. For the  $^1\text{H}$ -MAS experiments, 1,024 transients were collected with a recycle delay of 2 s. The proton  $90^\circ$  pulsewidth was 11  $\mu\text{s}$  and the experiments were collected with 59,970 complex data points and a sweepwidth of 59,970 Hz. The free induction decay (FID) of the  $^1\text{H}$ -MAS experiment was processed using backwards-linear prediction of the first three data points based on 256 points starting from the fourth data point. For the Fourier transformation, no weighting was applied. To correct for the amount of dissolved protein, the height of the TSST

spectra were normalized to that of the wild-type spectrum at 20°C.

## RESULTS

Standard homonuclear NMR techniques were used to obtain assignments of the amide and side-chain protons of wild-type and TSST type I AFP (data not shown). The high Ala content and repetitive  $\alpha$ -helical structure lead to considerable overlap of Ala resonances in the natural abundance  $^{15}\text{N}$ -HSQC and  $^{13}\text{C}$ -HSQC 2D NMR spectra [see Figs. 2(a) and 3(a)]. Nevertheless, residues from the N-terminus (Thr2, Ser4, Asp5), middle (Lys18, Glu22) and C-terminus (Thr35, Ala36, Arg37) were resolved well enough in order to analyze the two-dimensional (2D) solution NMR spectra. The top panel of Figure 2(a) shows a  $^{15}\text{N}$ -HSQC of wild-type type I AFP at 15, 5, and  $-5^\circ\text{C}$  with well-resolved resonances labeled with their residue identity. The amide proton and nitrogen chemical shifts of most residues *increase* as the temperature is lowered, with changes typically on the order of 0.1 ppm. This agrees with the general trend that  $^1\text{HN}$  chemical shifts, in the absence of large structural changes, increase as the temperature is lowered.<sup>37,38</sup> Two exceptions are the C-terminal residues Ala36 and Arg37. The chemical shift of Ala36 *decreases* by approximately 0.02 and that of Arg37 *decreases* by 0.2 ppm in the amide proton dimension. The pattern of changes in TSST as the temperature is lowered is almost identical to those seen for the wild-type protein [bottom panel of Fig. 2(a)]. The mutated residues Ser13/Ser24 are at a different amide proton and nitrogen chemical shift than that of Thr13/Thr24. Also, Ser13/Ser24 residues shift considerably less in the amide dimension than Thr13/Thr24 as the temperature is lowered (0.05 ppm versus 0.19 ppm).

To characterize differences between the wild-type and mutant TSST protein, an overlap of the  $^{15}\text{N}$ -HSQC spectra of the two proteins at  $-5^\circ\text{C}$  is shown in Figure 2(b). Residues located in the N- and C-termini of the proteins (Ser4, Asp5, Ala36, and Arg37) show perfect overlap. The largest difference occurs between Thr13/Thr24 and Ser13/Ser24 because of the change in the chemical nature of the side-chain (i.e., the change in chemical shift in this case does not reflect a change in conformation). Differences are observed involving residues Ala11, Leu12, Asn16/Asn27, and Glu22. This shows that the closer a residue is to the site of the mutation, the larger the difference in chemical shift from that of the wild-type protein. These results indicate that the wild-type and mutant proteins are similarly structured over the whole protein.

We subsequently used natural abundance  $^{13}\text{C}$ -NMR relaxation measurements at  $5^\circ$  and  $-1.2^\circ\text{C}$  in  $\text{D}_2\text{O}$  to examine whether there is any change in the dynamics of  $\text{C}\alpha$  atoms between the wild-type and mutant proteins. As with the  $^{15}\text{N}$ -HSQC data, the identifiable resonances in the  $^{13}\text{C}$ -HSQC spectra are non-Ala residues located over the whole structure. A temperature of  $-1.2^\circ\text{C}$  in  $\text{D}_2\text{O}$  represents an equivalent temperature to the  $-5^\circ\text{C}$  used for the  $^{15}\text{N}$ -HSQC collected in  $\text{H}_2\text{O}$  (i.e.,  $5^\circ\text{C}$  below the freezing point of the pure solvent). Comparing the spectra from the wild-type and mutant proteins, the major difference is

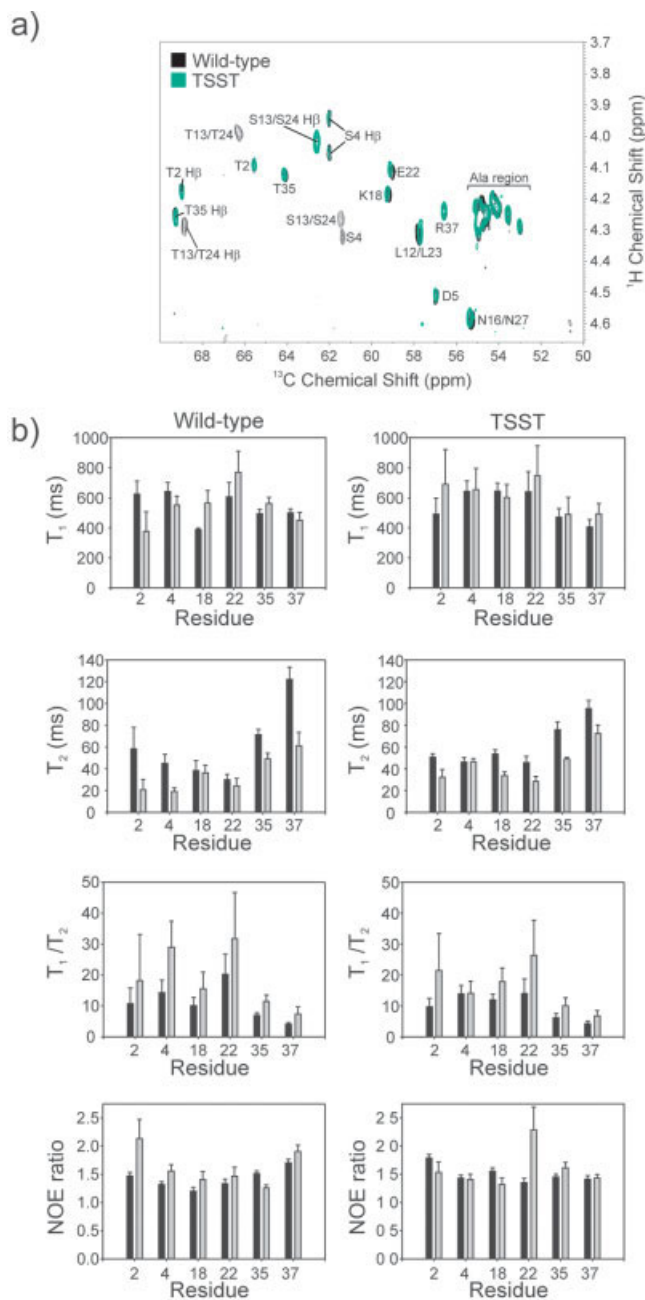


Fig. 3.  $^{13}\text{C}$  dynamics of type I AFP. **a**:  $\text{C}\alpha$  region of  $^{13}\text{C}$ -HSQC of wild-type and TSST type I AFP at  $5^\circ\text{C}$ . **b**: Heteronuclear  $^{13}\text{C}$ - $T_1$ ,  $^{13}\text{C}$ - $T_2$ ,  $^{13}\text{C}$ - $T_1/T_2$ , and  $\{^1\text{H}\}$ - $^{13}\text{C}$  NOE relaxation data of resolved resonances. Data were collected on samples dissolved in 99.9%  $\text{D}_2\text{O}$  at  $5^\circ\text{C}$  (black) and  $-1.2^\circ\text{C}$  (gray).

at the site of the mutation of Thr to Ser [Fig. 3(a)]. Unlike the overlapped  $^{15}\text{N}$ -HSQC spectra, however, only very small changes in chemical shift are observed for residues near the site of the mutations, showing that the backbone structure near the site of the mutations is unperturbed.

The natural-abundance relaxation data of well-separated resonances are shown in Figure 3(b). Decreasing the temperature had little effect on the  $T_1$  values. Similarly, making the Thr to Ser mutation had little effect on the

pattern of  $T_1$  values. Although  $T_1$  is 100–200 ms shorter for residues Thr35 and Arg37 compared with the other residues, the large experimental uncertainty makes it difficult to state whether this is meaningful. For the  $T_2$  data of both proteins, Thr35 and Arg37 show an average increase of 35 ms compared with residues Thr2 to Glu22. The NOE and  $T_1/T_2$  ratios at the two temperatures are shown in the bottom of Figure 3(b). In the absence of structural exchange, the  $T_1/T_2$  ratio is determined by the overall correlation time.<sup>39</sup> Lowering the temperature to  $-1.2^\circ\text{C}$  caused  $T_1/T_2$  to increase; this is expected because the protein will tumble more slowly (i.e.,  $T_1/T_2$  increases as the solution becomes more viscous). In the study of the apolipoprotein E peptide, it was found that the large  $T_1/T_2$  ratio was the result of the anisotropic motion of the helix while tumbling in solution, which was best described as a prolate ellipsoid.<sup>40</sup> Undertaking the same approach using our  $^{13}\text{C}$  natural abundance relaxation experiments, we can calculate the expected  $T_1$ ,  $T_2$ , and NOE values.<sup>41</sup> We assume that the diffusion tensor ratio of the long axis ( $D_{\parallel}$ ) to the short axis ( $D_{\perp}$ ) of the protein is equal to the ratio of the length of the rigid portion of the helix to its diameter. Type I AFP gives a  $D_{\parallel}:D_{\perp}$  of 7.2 when we define residues 2 to 29 as a rigid helix and assume the average side-chain to be an alanine residue. At  $5^\circ\text{C}$ , this gives a predicted  $T_1$  value of 465 ms, a predicted  $T_2$  value of 51.5 ms, and an NOE ratio of 1.19. Because these values are similar to the experimentally determined values, most of the  $\alpha$ -helix may be rigid, although data would be needed for residues 23 to 34 to provide confirmation. The C-terminal residues (Thr35 and Arg37) show larger  $T_2$  values than residues 2 to 22, whereas the NOE ratio remains fairly constant. The trends of these two residues are an expression of the reduced spectral density functions  $J(0)$  and  $J(\omega_0)$ , where  $J(\omega_0)$  (high-frequency function, i.e., fast internal motions) is reflected in the NOE ratio and  $T_2$  is dominated by  $J(0)$  (which is sensitive to motions on all time scales). This suggests that Thr35 and Arg37 may be more flexible than residues 2 to 22 at both temperatures for both wild-type and mutant proteins at both temperatures. The only apparent difference in the  $T_2$  values occurs between wild-type and TSST residue 4 at  $-1.2^\circ\text{C}$ . Because we found no other changes between these proteins in this or any other experiments, the difference is likely attributable to an error in measurement of  $T_2$ . Conclusive analysis of all of these data, however, will require isotopically labeled protein.

Although studies of AFP in the solution state have provided insight into the structure and dynamics of a single  $\alpha$ -helix, it is not known whether these data necessarily represent the structure and behavior of the protein when bound to ice. We therefore used  $^{13}\text{C}$ -CP/MAS and  $^{13}\text{C}$ -MAS experiments of  $^{13}\text{C}\alpha$  labeled Ala17 (wild-type AFP) or Ala21 (TSST) to follow the structure of the AFP in ice and solution, respectively.  $^{13}\text{C}\alpha$  chemical shifts are sensitive indicators of protein secondary structure,<sup>42</sup> and site-specific labeling allows us to follow the structure of a residue located on the Ala-rich face. The sample was frozen while spinning at a temperature of  $-5^\circ\text{C}$ . Ideally,

the sample should be frozen as a single ice crystal so as to mimic the binding of AFP to ice as it might occur in the fish.<sup>43</sup> However, this type of experiment is performed at a concentration of  $\sim 1$  versus 25 mg/mL for the solid-state NMR experiments, and would require impractical data collection times ( $>1$  year). Freezing the samples overnight at  $-5^\circ\text{C}$  allows the AFP to bind to nascent ice crystals in a manner that would inhibit ice growth at higher temperatures.

Freezing was verified by using the  $^{13}\text{C}$ -MAS experiment, wherein the  $^{13}\text{C}\alpha$  resonance is only observed from protein in the liquid state. Circular dichroism<sup>6,16,20</sup> and NMR<sup>44</sup> experiments have previously demonstrated that type I AFP becomes more  $\alpha$ -helical as it is cooled. The wild-type  $^{13}\text{C}\alpha$  chemical shift at  $20^\circ\text{C}$  is 54.6 ppm by  $^{13}\text{C}$ -MAS, which agrees with the previously determined value of 54.5 ppm by nonspinning  $^{13}\text{C}$ -NMR.<sup>44</sup> Similarly, the  $^{13}\text{C}\alpha$  chemical shift of TSST is 54.6 ppm by  $^{13}\text{C}$ -MAS and 54.4 ppm by nonspinning  $^{13}\text{C}$ -NMR. An additional peak is seen at  $\sim 18.5$  ppm in all experiments, which represents the natural abundance signal from the  $^{13}\text{C}\alpha$  atoms of the 23 Ala methyl groups. A  $^{13}\text{C}$ -CP/MAS study of various alanine polymers showed that  $^{13}\text{C}\beta$  atoms in an  $\alpha$ -helical conformation were at 17.1 ppm whereas atoms in a  $\beta$ -strand conformation were at 22.0 ppm (when corrected to DSS).<sup>45</sup> The natural abundance peak at 18.5 ppm in our experiments suggests that type I AFP may be  $\alpha$ -helical in ice over most of the protein.  $^{13}\text{C}$ -CP/MAS was subsequently used to examine the secondary structure of wild-type and TSST type I AFP when frozen in ice at  $-5^\circ\text{C}$ . The  $^{13}\text{C}\alpha$  chemical shift of both proteins was 56.6 ppm. This value is larger than that measured at  $5^\circ\text{C}$ , which shows that in ice both wild-type and mutant AFPs are even more  $\alpha$ -helical than in solution.

Because the backbone structural and solution relaxation data did not reveal any significant difference between the wild-type and TSST AFP, we used  $^1\text{H}$ -MAS to examine the behavior of these proteins at temperatures below the freezing point of the solution [Fig. 5(a)]. Unlike a previous protein  $^1\text{H}$ -MAS study,<sup>46</sup> sine-bell processing was not required to remove the residual HDO peak, which allows us to make quantitative comparisons between the spectra. When the temperature is lowered to  $3.8^\circ\text{C}$  (the freezing point of  $\text{D}_2\text{O}$ ), the intensity of the peaks between the proteins remains approximately equal. An expansion of the region from 0 to 2.5 ppm at  $1.8^\circ\text{C}$  and below is shown in Figure 5(b). The majority of the residual  $^1\text{H}$  signal in this region is from the 23 Ala methyl groups at  $\sim 1.4$  ppm. At  $1.8^\circ\text{C}$ , the signal from this region of the TSST mutant is approximately 1/3 that of the wild-type protein. As the temperature is lowered to  $0.0^\circ\text{C}$ , some signal remains with the wild-type sample, but there is almost no signal from the mutant. At  $-5.0^\circ\text{C}$ , neither protein shows any residual signal, showing that both proteins are completely immobilized once fully frozen in the ice at a temperature below the maximal ice-inhibitor activity (the thermal hysteresis point).

## DISCUSSION

Recent experiments have shown that the methyl groups of the type I AFP Ala residues are more important to the ice-binding interaction than the hydroxyl side-chains.<sup>16–18,21</sup> We examined here the behavior of wild-type protein AFP and the mutant TSST in water and ice to see if the differences in activity could be attributed to differences in the backbone structure or dynamics. The relatively small changes in the chemical shifts of the <sup>15</sup>N-HSQC and <sup>13</sup>C-HSQC spectra of wild-type and TSST type I AFP agrees with CD and NMR results that show that the proteins remain structured and the  $\alpha$ -helical content increases as the temperature of the solvent is lowered to near freezing temperatures<sup>20</sup> or to a super-cooled state.<sup>44</sup> However, not all of the identifiable resonances change to the same extent. The chemical shift changes of Ala36 and the terminal residue Arg37 are in the opposite direction to other residues, whereas Glu22 undergoes a very small shift. For the terminal residues, the change in direction of the chemical shift change may reflect the involvement of these residues in the cap structure, which is thought to stabilize the single  $\alpha$ -helix in solution.<sup>11,47</sup> For Glu22, the X-ray structure has shown that this residue is involved in a salt-bridge with residue Lys18, which may restrict the position of the residue such that its environment does not change as the protein becomes more  $\alpha$ -helical.

In the <sup>15</sup>N-HSQC 2D NMR spectra of the wild-type and mutant proteins [Fig. 2(b)], no large amide chemical shifts were observed as the temperature was lowered. A similar result was seen for the insect *Tenebrio molitor* AFP, where the lack of change was attributed to the AFP maintaining a rigid structure even at low temperatures.<sup>48</sup> The largest variation is observed between Thr13/Thr24 and Ser13/Ser24 in the <sup>15</sup>N-HSQC. However, the <sup>13</sup>C-HSQC spectra show that this change is attributable to the mutation of the residue and not a change in the backbone conformation. Most of the differences between the wild-type and mutant spectra can be correlated with the proximity of the residue to the site of the mutation. Residues within one  $\alpha$ -helical turn of the mutation (Ala11, Leu12, Ala15, and Ala26) showed the largest changes, whereas residues further away (Asn16/Asn27) showed smaller changes in amide chemical shift. Overall, these small differences suggest that the structure of TSST is very similar to the wild-type protein despite the loss of the two methyl groups of Thr13 and Th24. Figure 2(a) shows that the amide protons of Thr13/Thr24 undergo a much larger shift as the temperature is lowered compared with those in Ser13/Ser24, which show almost no change. In contrast, <sup>13</sup>C $\alpha$  chemical shift studies have shown that the  $\alpha$ -helicity of both wild-type and mutant protein change to the same extent as the solution is super-cooled.<sup>44</sup>

The natural abundance, {<sup>1</sup>H}-<sup>13</sup>C relaxation data were examined to see whether changes in the dynamics could explain differences in activity between the wild-type and TSST mutant AFPs (Fig. 3). Although Ala17 is <sup>13</sup>C $\alpha$  labeled in the wild-type protein and Ala21 is labeled in the TSST mutant, the residues experience very similar changes

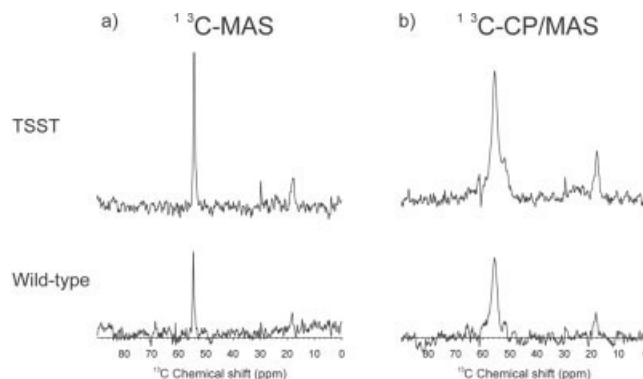


Fig. 4. <sup>13</sup>C-NMR spectra of wild-type and the mutant TSST type I AFP. **a:** Liquid state data were collected at 20°C using <sup>13</sup>C-MAS direct polarization experiment. The main peak shows the chemical shift of <sup>13</sup>C $\alpha$ -Ala17 for wild-type protein and <sup>13</sup>C $\alpha$ -Ala21 for the mutant. **b:** Solid-state data collected at -5°C using the <sup>13</sup>C-CP/MAS experiment.

in the chemical shift during cooling freezing, as was also shown in a previous study.<sup>44</sup> The flanking sequences are different in the two proteins (Ala Asn<sup>17</sup>Ala Lys Ala versus Ala Ala<sup>21</sup>Ala Glu Leu). Both labeled Ala residues are on the same face of the  $\alpha$ -helix. This suggests that the local sequence does not have a dramatic effect on the chemical shift of the <sup>13</sup>C $\alpha$ -Ala in this or subsequent experiments.

The data showed that both proteins consist of  $\alpha$ -helices that are rigid over residues 2 to 29, with the proteins becoming less rigid in the C-terminal region. Decreasing the temperature did not appreciably alter the rigidity of the center of the protein, despite the increase in  $\alpha$ -helical content.<sup>20,44</sup> The T<sub>2</sub> data suggest that Thr35 and Arg37 may be more flexible. This increased flexibility may explain the smaller loss in activity when the terminal threonines are mutated to serine. The substitution of Thr in the first and fourth positions (STTS) resulted in a TH activity of ~70% relative to wild-type protein,<sup>18</sup> compared with the 10% activity for TSST.<sup>16,18</sup> This result is reminiscent of the sbwAFP zipper model,<sup>49</sup> where the conservation of Thr residues led to the hypothesis that the conserved Thr rank bound ice first. A similar model can be proposed for type I AFP, where the rigid central Thr residues (Thr13/Thr24) may bind ice first, followed by the more flexible terminal Thr residues (Thr2/Thr35).

Whereas solution-state and X-ray studies have described the structure of type I antifreeze protein in detail, the crystallizations were performed in 83.3% acetone<sup>50</sup> while the NMR studies were performed in the absence of ice.<sup>20,44</sup> We therefore examined the structure of type I AFP and the TSST mutant at below freezing temperatures using solid-state NMR by following <sup>13</sup>C $\alpha$  chemical shifts. Figure 4 shows that the freezing of the sample caused both proteins to become even more  $\alpha$ -helical than in the solution state. This demonstrates that neither wild-type nor mutant type I AFP loses structure in the presence of ice, and that the backbone structure determined by crystallography and NMR is representative of the ice-bound structure. Examination of type I AFP in ice by scanning tunneling microscopy agrees with this observation.<sup>51</sup> Grooves in the STM surface plot are consistent with one type I AFP

molecule bound at approximately equal intervals. The length of the groove ( $\sim 60$  Å) is similar to the length of the helical type I AFP ( $\sim 50$  Å), which shows that the protein is not bound in an extended conformation.

Because the structures become more  $\alpha$ -helical in ice, it is possible that type I AFP shows more bending at elevated temperatures. In addition, the absence of two methyl groups in the TSST protein may increase bending of the helix relative to the wild-type protein, such that the mutant protein is not able to make an effective match to the ice lattice. This would manifest itself experimentally in motions on the microsecond to millisecond timescale, which is not directly observed in our experiments (Fig. 3). In a previous article,<sup>44</sup> we measured the  $^{13}\text{C}$ - $T_2$  of wild-type and mutant TSST at three magnetic field strengths (300, 600, and 800 MHz), over a temperature range of 20 to  $-5^\circ\text{C}$  and in  $\text{D}_2\text{O}$  and  $\text{H}_2\text{O}$ . The plot of  $^{13}\text{C}$ - $T_2$  versus viscosity/temperature was linear for both proteins and under all conditions. This linearity demonstrates that the wild-type and mutant proteins did not undergo any exchange broadening, and that they do not show appreciable bending of the  $\alpha$ -helix over the temperatures examined.

Because the backbone of wild-type and TSST type I AFP are equally structured in ice and the  $^{13}\text{C}\alpha$  backbone dynamics in solution are similar, we examined side-chain protons in water and ice using  $^1\text{H}$ -MAS NMR.<sup>46</sup> Figure 5 shows that the TSST sample loses signal somewhat faster than the wild-type protein until  $-5.0^\circ\text{C}$  is reached (i.e.,  $8.8^\circ\text{C}$  below the freezing point of  $\text{D}_2\text{O}$ ), at which point both samples show almost no signal. A previous study demonstrated that the wild-type and mutant AFPs partition equally between the solution and solid phases,<sup>52</sup> showing that the lack of activity in TSST is not the result of a “freeze concentration” effect. Therefore, the difference in the  $^1\text{H}$ -MAS spectra, although small, is not caused by reduced partitioning of TSST in ice. It is possible that this difference may represent the optimal positioning of the methyl groups in order to dock to ice or to ensure maximum shape complementarity, or to ensure removal of bound water from the protein before binding to ice. However, this hypothesis requires more experimental evidence.

## CONCLUSION

The elucidation of AFP activity has not been straightforward, and requires that experiments that may seem to be confirmatory to be performed. The ice-binding models presented in previous research all assumed that the structure of type I AFP is the same in solution as when it is in ice. We have shown here that type I AFP does not undergo cold-denaturation when frozen in ice. We also demonstrated that the mutant TSST remains similarly structured whether in solution or in ice, showing that its activity loss is not attributable to any subtle change in the structure or dynamics of the protein. Careful examination of the surface properties of both AFP and ice may provide new models of this protein’s enigmatic mechanism.

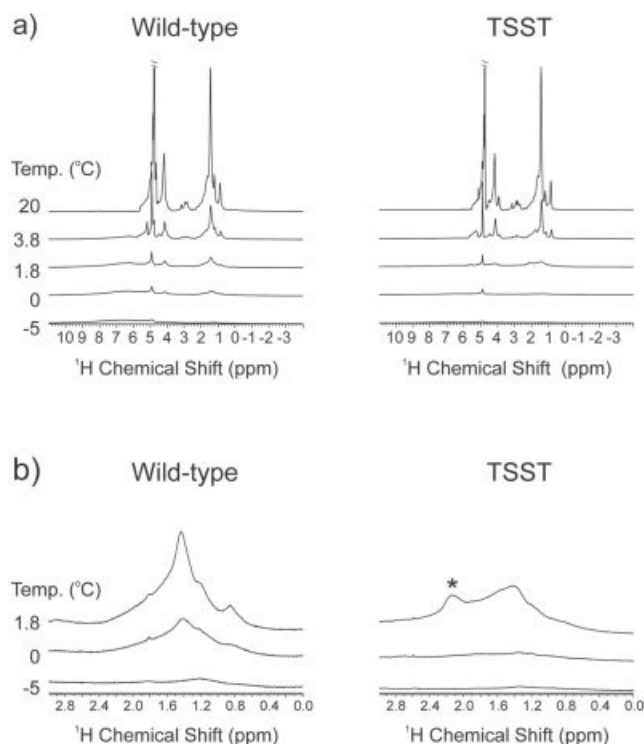


Fig. 5.  $^1\text{H}$ -NMR spectra of wild-type and the mutant TSST type I AFP using  $^1\text{H}$ -MAS. Samples were dissolved in 99.9%  $\text{D}_2\text{O}$ . **a:** Spectra of the entire sweepwidth. The HDO peak has been truncated. The vertical scale is constant between each temperature change. **b:** Expansion of the region from 0.0 to 3.0 ppm. Spectra are shown at a constant scale between each temperature but the vertical scale is magnified 10 times compared with (a). The asterisk marks a peak that is not seen in other TSST spectra, and is likely an artifact.

## ACKNOWLEDGMENTS

The authors thank Jennifer Labrecque and Marc Genest for synthesis of the AFP peptides, and Leo Spyropoulos for help calculating the anisotropic rotational correlation times and backbone  $^1\text{H}$ - $^{13}\text{C}$  NMR relaxation parameters. They also thank the Canadian National High Field NMR Centre (NANUC) for their assistance and use of the 800-MHz spectrometer. Operation of NANUC is funded by the Canadian Institutes of Health Research (CIHR), the Natural Science and Engineering Research Council of Canada (NSERC), and the University of Alberta. This work is supported by grants from the CIHR, the Government of Canada’s Network of Centres of Excellence program (supported by CIHR and NSERC through the Protein Engineering Network of Centres of Excellence, Inc.) to BDS. SPG is the recipient of a CIHR Fellowship and an Alberta Heritage Fund for Medical Research Fellowship.

## REFERENCES

- Zachariassen KE, Kristiansen E, Pedersen SA, Hammel HT. Ice nucleation in solutions and freeze-avoiding insects-homogeneous or heterogeneous? *Cryobiology* 2004;48:309–321.
- Wilson PW, Leader JP. Stabilization of supercooled fluids by thermal hysteresis proteins. *Biophys J* 1995;68:2098–2107.
- Raymond JA, DeVries AL. Adsorption inhibition as a mechanism of freezing resistance in polar fishes. *Proc Natl Acad Sci USA* 1977;74:2589–2593.

4. Ba Y, Wongsakhaluang J, Li J. Reversible binding of the HPLC6 isoform of type I antifreeze proteins to ice surfaces and the antifreeze mechanism studied by multiple quantum filtering-spin exchange NMR experiment. *J Am Chem Soc* 2003;125:330–331.
5. Ben RN. Antifreeze glycoproteins: preventing the growth of ice. *ChemBiochem* 2001;2:161–166.
6. Harding MM, Anderberg PI, Haymet AD. 'Antifreeze' glycoproteins from polar fish. *Eur J Biochem* 2003;270:1381–1392.
7. Haymet AD, Ward LG, Harding MM. Hydrophobic analogues of the winter flounder 'antifreeze' protein. *FEBS Lett* 2001;491:285–288.
8. Sönnichsen FD, Davies PL, Sykes BD. NMR structural studies on antifreeze proteins. *Biochem Cell Biol* 1998;76:284–293.
9. Jia Z, Davies PL. Antifreeze proteins: an unusual receptor-ligand interaction. *Trends Biochem Sci* 2002;27:101–106.
10. Graether SP, Sykes BD. Cold survival in freeze-intolerant insects. *Eur J Biochem* 2004;271:3285–3296.
11. Sicheri F, Yang DS. Ice-binding structure and mechanism of an antifreeze protein from winter flounder. *Nature* 1995;375:427–431.
12. Yang DS, Sax M, Chakrabarty A, Hew CL. Crystal structure of an antifreeze polypeptide and its mechanistic implications. *Nature* 1988;333:232–237.
13. DeVries AL, Lin Y. Structure of a peptide antifreeze and mechanism of adsorption to ice. *Biochim Biophys Acta* 1977;495:388–392.
14. Knight CA, Cheng CC, DeVries AL. Adsorption of alpha-helical antifreeze peptides on specific ice crystal surface planes. *Biophys J* 1991;59:409–418.
15. Wen D, Laursen RA. A model for binding of an antifreeze polypeptide to ice. *Biophys J* 1992;63:1659–1662.
16. Chao H, Houston ME, Hodges RS, et al. A diminished role for hydrogen bonds in antifreeze protein binding to ice. *Biochemistry* 1997;36:14652–14660.
17. Haymet AD, Ward LG, Harding MM, Knight CA. Valine substituted winter flounder 'antifreeze': preservation of ice growth hysteresis. *FEBS Lett* 1998;430:301–306.
18. Zhang W, Laursen RA. Structure-function relationships in a type I antifreeze polypeptide. The role of threonine methyl and hydroxyl groups in antifreeze activity. *J Biol Chem* 1998;273:34806–34812.
19. Sönnichsen FD, DeLuca CI, Davies PL, Sykes BD. Refined solution structure of type III antifreeze protein: hydrophobic groups may be involved in the energetics of the protein-ice interaction. *Structure* 1996;4:1325–1337.
20. Gronwald W, Chao H, Reddy DV, Davies PL, Sykes BD, Sönnichsen FD. NMR characterization of side chain flexibility and backbone structure in the type I antifreeze protein at near freezing temperatures. *Biochemistry* 1996;35:16698–16704.
21. Baardsnes J, Kondejewski LH, Hodges RS, Chao H, Kay C, Davies PL. New ice-binding face for type I antifreeze protein. *FEBS Lett* 1999;463:87–91.
22. Yang DS, Hon WC, Bubanko S, et al. Identification of the ice-binding surface on a type III antifreeze protein with a "flatness function" algorithm. *Biophys J* 1998;74:2142–2151.
23. Jorov A, Zhorov BS, Yang DS. Theoretical study of interaction of winter flounder antifreeze protein with ice. *Protein Sci* 2004;13:1524–1537.
24. Yang C, Sharp KA. Hydrophobic tendency of polar group hydration as a major force in type I antifreeze protein recognition. *Proteins* 2005;59:266–274.
25. Graether SP, Slupsky CM, Sykes BD. Freezing of a fish antifreeze protein results in amyloid fibril formation. *Biophys J* 2003;84:552–557.
26. Hodges RS, Semchuk PD, Taneja AK, Kay CM, Parker JM, Mant CT. Protein design using model synthetic peptides. *J Pept Res* 1988;1:19–30.
27. Wishart DS, Bigam CG, Yao J, et al.  $^1\text{H}$ ,  $^{13}\text{C}$ , and  $^{15}\text{N}$  chemical shift referencing in biomolecular NMR. *J Biomol NMR* 1995;6:135–140.
28. Muhandiram DR, Kay LE. Gradient-enhanced triple-resonance 3-dimensional NMR experiments with improved sensitivity. *J Magn Reson B* 1994;103:203–216.
29. Kay LE, Keifer P, Saarinen T. Pure absorption gradient enhanced heteronuclear single quantum correlation spectroscopy with improved sensitivity. *J Am Chem Soc* 1992;114:10663–10665.
30. Kumar A, Ernst RR, Wuthrich K. A two-dimensional nuclear Overhauser enhancement (2D NOE) experiment for the elucidation of complete proton-protein cross-relaxation networks in biological macromolecules. *Biochem Biophys Res Commun* 1980;95:1–6.
31. Marion D, Kay LE, Sparks SW, Torchia DA, Bax A. 3-Dimensional heteronuclear NMR of N-15 labeled proteins. *J Am Chem Soc* 1989;111:1515–1517.
32. Farrow NA, Muhandiram R, Singer AU, et al. Backbone dynamics of a free and phosphopeptide-complexed Src homology 2 domain studied by  $^{15}\text{N}$  NMR relaxation. *Biochemistry* 1994;33:5984–6003.
33. Johnson BA, Blevins RA. NMR VIEW: a computer-program for the visualization and analysis of NMR data. *J Biomol NMR* 1994;4:603–614.
34. Gagné SM, Tsuda S, Spyrapoulos L, Kay LE, Sykes BD. Backbone and methyl dynamics of the regulatory domain of troponin C: anisotropic rotational diffusion and contribution of conformational entropy to calcium affinity. *J Mol Biol* 1998;278:667–686.
35. Van Geet AL. Calibration of methanol nuclear magnetic resonance thermometer at low temperature. *Anal Chem* 1970;42:679.
36. Raiford DS, Fisk CL, Becker ED. Calibration of methanol and ethylene-glycol nuclear magnetic-resonances thermometers. *Anal Chem* 1979;51:2050–2051.
37. Andersen NH, Neidigh JW, Harris SM, Lee GM, Liu ZH, Tong H. Extracting information from the temperature gradients of polypeptide NH chemical shifts.1. The importance of conformational averaging. *J Am Chem Soc* 1997;119:8547–8561.
38. Merutka G, Dyson HJ, Wright PE. 'Random coil'  $^1\text{H}$  chemical shifts obtained as a function of temperature and trifluoroethanol concentration for the peptide series GGXGG. *J Biomol NMR* 1995;5:14–24.
39. Kay LE, Torchia DA, Bax A. Backbone dynamics of proteins as studied by  $^{15}\text{N}$  inverse detected heteronuclear NMR spectroscopy: application to staphylococcal nuclease. *Biochemistry* 1989;28:8972–8979.
40. Raussens V, Slupsky CM, Sykes BD, Ryan RO. Lipid-bound structure of an apolipoprotein E-derived peptide. *J Biol Chem* 2003;278:25998–26006.
41. Cantor CR, Schimmel PR. Size and shape of macromolecules. In: *Techniques for the study of biological structure and function*. San Francisco: W.H. Freeman and Company; 1980. 590 p.
42. Wishart DS, Sykes BD, Richards FM. Relationship between nuclear magnetic resonance chemical shift and protein secondary structure. *J Mol Biol* 1991;222:311–333.
43. Harding MM, Ward LG, Haymet AD. Type I 'antifreeze' proteins. Structure-activity studies and mechanisms of ice growth inhibition. *Eur J Biochem* 1999;264:653–665.
44. Graether SP, Slupsky CM, Davies PL, Sykes BD. Structure of type I antifreeze protein and mutants in supercooled water. *Biophys J* 2001;81:1677–1683.
45. Saito H. Conformation-dependent C-13 chemical-shifts: a new means of conformational characterization as obtained by high-resolution solid-state C-13 Nmr. *Magn Reson Chem* 1986;24:835–852.
46. Volke F, Pampel A, Haensler M, Ullmann G. Proton MAS NMR of a protein in a frozen aqueous solution. *Chem Phys Lett* 1996;262:374–378.
47. Low WK, Lin Q, Hew CL. The role of N and C termini in the antifreeze activity of winter flounder (*Pleuronectes americanus*) antifreeze proteins. *J Biol Chem* 2003;278:10334–10343.
48. Daley ME, Graether SP, Sykes BD. Hydrogen bonding on the ice-binding face of a  $\beta$ -helical antifreeze protein indicated by amide proton NMR chemical shifts. *Biochemistry* 2004;43(41):13012–13017.
49. Doucet D, Tyshenko MG, Kuiper MJ, et al. Structure-function relationships in spruce budworm antifreeze protein revealed by isoform diversity. *Eur J Biochem* 2000;267:6082–6088.
50. Yang DS, Chung YJ, Chen P, Rose JP, Hew CL. Single crystals of a winter flounder antifreeze polypeptide. *J Mol Biol* 1986;189:725.
51. Grandum S, Yabe A, Nakagomi K, et al. Analysis of ice crystal growth for a crystal surface containing adsorbed antifreeze proteins. *J Cryst Growth* 1999;205:382–390.
52. Marshall CB, Tomczak MM, Gauthier SY, et al. Partitioning of fish and insect antifreeze proteins into ice suggests they bind with comparable affinity. *Biochemistry* 2004;43:148–154.